Monatsh Chem (2014) 145:593–603
DOI 10.1007/s00706-013-1113-5

ORIGINAL PAPER

Theoretical and experimental study of the protonated 2,4,6-tri(2-pyridyl)-1,3,5-triazine $[TPTZH_2]^{2+}$

Hassan Hadadzadeh · Matthias Weil · Mahbobeh Maghami · Marzieh Daryanavard · Mahbod Morshedi · Aliakbar Dehno Khalaji

Received: 23 May 2013 / Accepted: 24 October 2013 / Published online: 26 November 2013
© Springer-Verlag Wien 2013

Abstract The reaction between 2,4,6-tri(2-pyridyl)-1,3,5-triazine (TPTZ) and sulfuric acid in the presence of NH_4PF_6 yielded crystals of $[TPTZH_2](PF_6)_2{\cdot}H_2O$, characterized by spectroscopic methods and single-crystal X-ray diffraction. The structural data indicate that the diprotonated form, $[TPTZH_2]^{2+}$, is more planar than the neutral TPTZ molecule. Due to the presence of PF_6^- anions located between neighboring dications, the triazine and/or pyridyl rings in each dication cannot interact in a π–π fashion. The proton affinity of TPTZ was computed using density function theory (B3LYP hybrid functional). Calculated thermochemical results and proton affinities indicate that for the first protonation, the favorable N atoms are different from those obtained from calculations based on Merz-Kollman atomic charges. For the second protonation, the proton affinities show a clear preference of the protonation on two N atoms, this time not contradicted by Merz-Kollman atomic charges, and in agreement with the experimental data. In the UV–Vis spectrum, two visible absorption bands of $[TPTZH_2](PF_6)_2{\cdot}H_2O$ are most likely arising from an outer-sphere charge-transfer. The photoluminescence properties of TPTZ and $[TPTZH_2](PF_6)_2$ were studied at room temperature in CH_3CN solution.

Keywords Proton affinity · Merz-Kollman atomic charges · 2,4,6-Tri(2-pyridyl)-1,3,5-triazine · DFT · Crystal structure

H. Hadadzadeh (✉) · M. Maghami · M. Daryanavard
Department of Chemistry, Isfahan University of Technology, 84156-83111 Isfahan, Iran
e-mail: hadad@cc.iut.ac.ir

M. Weil
Division of Structural Chemistry, Institute of Chemical Technologies and Analytics, Vienna University of Technology, Getreidemarkt 9/164-SC, 1060 Vienna, Austria

M. Morshedi
Research School of Chemistry, Australian National University, Canberra, ACT 0200, Australia

A. D. Khalaji
Department of Chemistry, Faculty of Science, Golestan University, Gorgan, Iran

Introduction

Proton affinity (PA) and protonation reactions are of considerable interest in all areas of chemistry. The PA of an atom or molecule is the energy released upon reaction of this species with a proton in the gas phase. There is a relationship between orbital energies and the energy released when a proton attacks the highest occupied molecular orbital (HOMO) of a certain Lewis base. Protonation alters many physical and chemical properties beyond the changes in mass and charge. Transfer of protons can be regarded as one of the simplest, but very important, chemical signals. For example, many life processes, such as enzymes, only work within a very narrow pH range [1].

Heterocyclic systems are of widespread occurrence in nature, particularly in such natural products as nucleic acids, plant alkaloids, vitamins, proteins, anthocyanins, flavones, heme pigments, chlorophyll, and the building blocks of many antibiotics, anticancer agents, fungicides, and several other drugs [1–7].

In polybasic compounds in which the species can undergo more than one protonation, the determination of the protonation sites and of the PA of gas and solution phases of aromatic heterocyclic compounds is of

importance and has attracted considerable interest for years. Theoretical and experimental studies on the protonation of polypyridine molecules are also of great interest in pharmacological and biological research since the site of protonation is closely related to the expression of biological activity. In addition, protonated N-heterocyclic compounds play an important role as intermediates in many catalytic reactions. One of the most important representatives of an N-heterocycle is pyridine. The lone pair of electrons on the nitrogen atom in pyridine behaves differently and can react with different chemical species: (1) Brønsted acids give salts; (2) Lewis acids form coordination compounds; (3) transition metal ions undergo complex formation; (4) reactive halides give quaternary salts; (5) halogens form adducts; (6) certain oxidizing agents yield amine oxides; (7) aminating agents give N-amino derivatives very similar to that in trimethylamine or other tertiary amines and react under mild conditions with electrophilic reagents. In addition, pyridine contains a basic nitrogen atom and upon protonation, forms the pyridinium cation that retains the pyridine aromaticity [7, 8].

In recent years, computational chemistry has played an important role of supporting and supplementing the experimental research of protonated N-heterocyclic compounds. Nevertheless, the prediction of the correct site for protonation is still a challenging problem from a theoretical perspective. For instance, the PAs of pyridine, imidazole, and pyrazole derivatives have been calculated using an ab initio quantum mechanical method, with various double zeta and triple zeta basis sets in combination with the Poisson-Boltzmann continuum solvation model by Hwang et al. [9]. Huang and Rodgers [10] reported the PAs of pyrrole, pyrazole, and imidazole at the Møller-Plesset (MP2) level of theory. Schmiedekamp et al. [11] reported density functional theory (DFT) calculations on a series of triazoles.

The goal of this work is to obtain a detailed insight into the protonation of 2,4,6-tri(2-pyridyl)-1,3,5-triazine (TPTZ) (Scheme 1) using both experimental methods (such as X-ray crystallography and spectroscopic techniques) and theoretical calculations.

Scheme 1

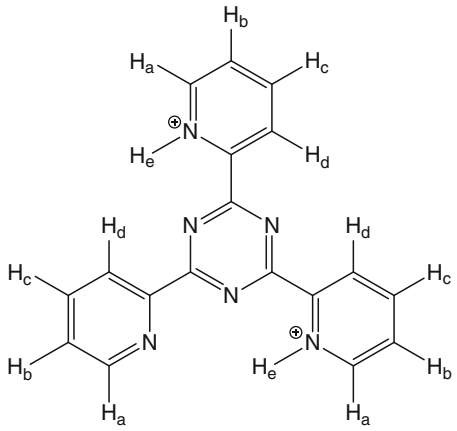

Results and discussion

Proton affinity and protonation sites

The proton affinity (PA) is considered as the negative enthalpy of the protonation reaction. Computed enthalpies for TPTZ together with its protonated forms at the most accessible N atoms (N5, N4, N6) are reported in Table 1. Since experimental data are not available so far, we cannot compare these computed PAs with measured data. Compounds reported in Scheme 2 present more than one protonation site. Due to the polybasicity of TPTZ, we have investigated PAs for all non-equivalent N atoms in order to evaluate the basicity and nucleophilic ability of each site. The high basicity of these protonation sites is related to the strong intramolecular N–H···N hydrogen bond which is formed upon protonation of N atoms.

In Table 2 selected optimized structural parameters of TPTZ, $[TPTZH]^+$, and $[TPTZH_2]^{2+}$ are reported. It is interesting to note that protonation makes every studied system flatten (Table 3). The added H atom is located between two N atoms so that an intramolecular N–H···N hydrogen bond occurs; in other words, a flat ring made up of C–N–H···N–C interactions that allow a strong intramolecular N–H···N hydrogen bond with a smaller N···N distance (Table 2) than a bent ring system. As it can be seen from Table 2, the bond lengths within the rings reflect the proton changes according to the Gutmann principles (Scheme 3) [12, 13]. Other bond lengths remain approximately the same.

Thermochemical results and the calculated PAs shown in Table 1 indicate that for the first protonation, the most favorable N atoms are N4 > N5 > N6. However, these results are contradicted by Merz-Kollman atomic charges showing the charge distribution to be N5 < N4 < N6 (Table 4). Considering the molecular orbitals of TPTZ, again one can deduce that the N4 site is the most accessible protonation site since the HOMO is concentrated on this atom (Fig. 1). Regrettably, not having any experimental data of the mono protonated $[TPTZH]^+$, we cannot conclude reliably which site will eventually accept the first proton.

After the first protonation, deciding which N atom is more accessible for the second protonation, becomes easier. It can be seen that after the first protonation on either N5 or N4, the HOMO is concentrated on N6. The

Table 1 Thermochemical values calculated for TPTZ and the protonated species

Energy (hartree)	TPTZ	N6	N4	N5	N6,4	N6,5	N4,5
E_{tot}	−1,021.903784	−1,022.29	−1022.3	−1,022.3	−1,022.59	−1,022.6	−1,022.59
$E_{tot} + ZPE_{tot}$	−1,021.633672	−1,022.01	−1,022.02	−1,022.02	−1,022.3	−1,022.3	−1,022.29
$E_{tot} + U_{tot}$	−1,021.615766	−1,021.99	−1,022.01	−1,022	−1,022.28	−1,022.28	−1,022.27
$E_{tot} + H_{tot}$	−1,021.614822	−1,021.99	−1,022	−1,022	−1,022.28	−1,022.28	−1,022.27
$E_{tot} + G_{tot}$	−1,021.683685	−1,022.06	−1,022.07	−1,022.06	−1,022.34	−1,022.35	−1,022.34
PA		238.7993	246.3894	241.5715	179.9012	181.0734	166.9397

Scheme 2

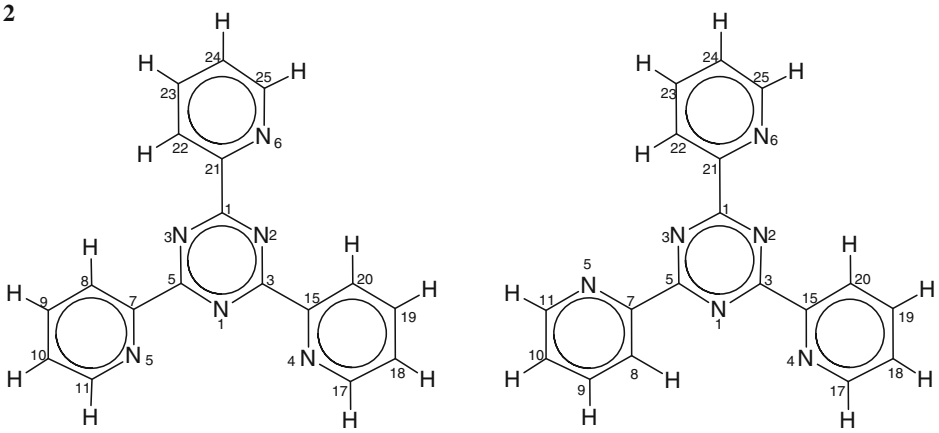

Conformation **A** Conformation **B**

PAs in Table 1 reveal that the protonation on N5 and N6 is more favorable than the other two protonation sites (N5–N4 or N4–N6, respectively). This time the obtained results are not contradicted by Merz-Kollman atomic charges, and are in agreement with the experimental data (Table 5).

Synthesis, crystal structure, and spectroscopic properties

The diprotonated form of 2,4,6-tris(2-pyridyl)-1,3,5-triazine, $[TPTZH_2]^{2+}$, was synthesized in good yield as the hexafluorophosphate salt (Scheme 4). The PF_6^- counterion increased the solubility of the salt in polar organic solvents and resulted in an easier purification. The salt was crystallized with one molecule of water. The molecular structure of the $[TPTZH_2]^{2+}$ cation together with the solvent water molecule and the two PF_6^- counteranions is shown in Fig. 2.

Hydrogen bonds are essential for the structural stability of many crystals. The analysis of hydrogen bond patterns for structures compiled in the Cambridge structural database (CSD) reveals some preferred hydrogen-bond motifs and hydrogen-bond selectivity for certain functional groups [14, 15]. The dication, $[TPTZH_2]^{2+}$, which arises from the protonation of the two pyridyl rings (C(7)–C(11)/N(5) and C(21)–C(25)/N(6)), shows a conformation imposed by two hydrogen bonding interactions with the solvent water molecule, (N5···O1 = 2.6568(16) Å, O1···N4 = 2.8760(17) Å; Table 6) situated coplanar with the triazine moiety; the torsion angle of N(1)–H(W1)–O(1)–N(5) is 0.32°, and the dihedral angle between the mean planes of water and triazine ring is 0.047°. As shown in Fig. 2, there are two crystallographically different PF_6^- anions in the structure. One of the two PF_6^- counteranions interacts with the $[TPTZH_2]^{2+}$ cation via an F···H–N hydrogen bond and the other with the solvent water molecule (Table 6). Due to the presence of the PF_6^- counteranions located between neighboring $[TPTZH_2]^{2+}$ cations, the triazine and/or pyridyl rings in each cation cannot interact in a $\pi\cdots\pi$ fashion (Fig. 3). Non-classical weak hydrogen bonding involving C(24)–H(24)···π(C(15,17–20)N4 ring) (2.885 Å) is also observed. Such a short intermolecular CH···π distance (<3.0 Å) is an indication for the occurrence of weak C–H···π hydrogen bonds [16, 17].

The crystal structures of the two neutral triazine isomers TPTZ and 2,4,6-tris(4-pyridyl)-1,3,5-triazine have been reported [18, 19]. The neutral TPTZ molecule is non-planar

Table 2 Calculated bond lengths/Å of TPTZ and the protonated species

Bond	TPTZ	N5	N4	N6	N6,5	N4,5	N5,6
C1–C21	1.496	1.486	1.485	1.488	1.489	1.469	1.489
C1–N2	1.331	1.334	1.349	1.330	1.328	1.347	1.344
C1–N3	1.339	1.355	1.340	1.321	1.336	1.353	1.322
C9–C10	1.391	1.397	1.390	1.390	1.393	1.395	1.389
C10–C11	1.396	1.384	1.398	1.399	1.387	1.383	1.403
C11–N5	1.331	1.343	1.330	1.329	1.342	1.347	1.327
C15–C20	1.401	1.399	1.386	1.398	1.399	1.387	1.383
C15–N4	1.339	1.343	1.351	1.339	1.345	1.354	1.356
C17–C18	1.396	1.399	1.383	1.398	1.403	1.383	1.387
C18–C19	1.391	1.390	1.398	1.390	1.389	1.396	1.393
C19–C20	1.390	1.392	1.394	1.392	1.392	1.396	1.399
C21–C22	1.400	1.399	1.399	1.387	1.385	1.401	1.385
C21–N6	1.339	1.341	1.341	1.351	1.355	1.346	1.355
C22–C23	1.39	1.392	1.392	1.393	1.398	1.392	1.397
C3–C17	1.496	1.482	1.487	1.486	1.472	1.489	1.490
C3–N1	1.335	1.346	1.328	1.332	1.345	1.346	1.320
C23–C24	1.391	1.389	1.390	1.398	1.394	1.389	1.395
C24–C25	1.395	1.399	1.399	1.382	1.386	1.404	1.385
C25–N6	1.332	1.329	1.330	1.345	1.344	1.326	1.346
C5–C7	1.496	1.489	1.485	1.485	1.489	1.490	1.469
C5–N3	1.340	1.322	1.337	1.355	1.337	1.320	1.351
C7–C8	1.400	1.386	1.398	1.400	1.383	1.386	1.400
C7–N5	1.338	1.352	1.342	1.340	1.356	1.354	1.346
C8–C9	1.390	1.394	1.392	1.392	1.399	1.396	1.392
N4–C17	1.331	1.330	1.344	1.330	1.327	1.348	1.341
N2–C3	1.340	1.336	1.320	1.352	1.352	1.316	1.338
N1–C5	1.333	1.327	1.344	1.334	1.322	1.345	1.347
N1–N5	2.772	2.586	2.720	2.737	2.611	2.735	2.700
N1–N4	2.761	2.732	2.612	2.760	2.693	2.770	2.595
N2–N6	2.755	2.725	2.721	2.635	2.668	2.704	2.695
N5–H	–	1.032	–	–	1.027	1.018	–
N4–H	–	–	1.030	–	–	–	1.029
N6–H	–	–	–	1.026	1.022	1.017	1.02
N5···N1	2.772	2.586	2.720	2.737	2.611	2.735	2.700
N4···N1	2.761	2.732	2.612	2.760	2.693	2.770	2.595
N6···N2	2.725	2.725	2.721	2.635	2.668	2.704	2.695

in the crystal, due to the steric effect of lone-pair electrons at the N atoms in both pyridyl and triazine rings, but the triazine ring and the three pyridyl rings are planar [19]. The ring orientations of the three pyridyl moieties with respect to the central triazine ring can be described by the dihedral angles between these rings. For the $[TPTZH_2]^{2+}$ cation, the pyridyl and triazine rings are nearly coplanar. The dihedral angles between the triazine ring (C(1)–N(2)–C(3)–N(1)–C(5)–N(3)) and each of the pyridyl rings (C(7)–C(11)/N(5), C(15)–C(17)/N(4), and C(21)–C(25)/N(6)) are 7.84°, 3.70°, and 6.19°, respectively. The C–N bond lengths within the pyridyl rings and the central triazine ring are nearly the same within experimental errors. The C–N distances are between 1.3320 (18) and 1.3428 (18) Å in the triazine ring in $[TPTZH_2]^{2+}$ and are approximately the same as in the neutral TPTZ molecule (1.334 (2)–1.350 (3) Å). The orientation of the pyridyl rings with respect to the pyrazine ring in the neutral and diprotonated TPTZ is represented in Scheme 5. As can be seen, due to the protonation, $[TPTZH_2]^{2+}$ is flatter (the root-mean-square deviation of the 24 atoms that define the ring system is 0.070 Å, with a maximal deviation of 0.1322 (13) Å for atom C10) than for the neutral TPTZ.

Predominant vibrational modes for $[TPTZH_2](PF_6)_2{\cdot}H_2O$ are associated with ν(N–H), ν(C=C), ν(C=N), ν(P–F), and ring stretching. The reported separation between ν(C=C) and ν(C=N) is close to 20 cm^{-1} for polypyridyl compounds [20–22] and thus the observed vibrational absorption bands for $[TPTZH_2]^{2+}$ at 1,539, 1,523, and 1,476 cm^{-1} may be due to either different ν(C=N) vibrations on the triazine and pyridyl rings or ν(C=C) and ν(C=N) with coincidental equivalence of the different aromatic rings. An intense band at 1,377 cm^{-1} is assigned to ring stretching of both triazine and pyridyl rings. The strong absorption band at 842 cm^{-1} is assigned to ν(P–F).

The results obtained from the ^{1}H NMR solution spectra support the results of the crystal structure analysis and suggest that the structure of the $[TPTZH_2]^{2+}$ cation is retained in DMSO-d_6 solution. The ideal symmetry of the TPTZ molecule in solution is D_{3h} and this molecule shows four well-resolved ^{1}H NMR signals (7.55, 8.80, 8.90, and 8.98 ppm) at room temperature [23]. In comparison, a small downfield shift (0.01–0.39 ppm) for all pyridyl protons of the $[TPTZH_2]^{2+}$ cation is observed. Different to the solid state structure of $[TPTZH_2](PF_6)_2{\cdot}H_2O$, the ^{1}H NMR spectrum of $[TPTZH_2]^{2+}$ in DMSO-d_6 shows that the two protons of the N^+–H bonds are equivalent and appear at 7.28 ppm.

The neutral TPTZ molecule has three intense absorption bands in the ultraviolet region, two $\pi \rightarrow \pi^*$ (204 (ε = 34,037 M^{-1} cm^{-1}) and 282 (ε = 44,035 M^{-1} cm^{-1}) nm) and one $n \rightarrow \pi^*$ (246 (ε = 29,178 M^{-1} cm^{-1}) nm) transition (Fig. 4a). The electronic spectrum of $[TPTZH_2](PF_6)_2{\cdot}H_2O$ was measured in CH_3CN solution (Fig. 4b). The intense absorption bands at 245 nm (ε = 44,580 M^{-1} cm^{-1}) and 280 nm (ε = 59,360 M^{-1} cm^{-1}) are assigned to $n \rightarrow \pi^*$ and $\pi \rightarrow \pi^*$ transitions, respectively. When the electronic spectrum of $[TPTZH_2]^{2+}$ was recorded in the presence of excess H_2SO_4, the absorption band ($n \rightarrow \pi^*$) at 245 nm disappeared. Unlike the colorless solution of the neutral TPTZ in acetonitrile, the acetonitrile solution of $[TPTZH_2](PF_6)_2{\cdot}H_2O$ is violet,

Table 3 Calculated torsion angles/° of TPTZ and the protonated species

Bond	TPTZ	N5	N4	N6	N4,6	N4,5	N6,5
N2–C1–C21–N6	−10.33	−0.06	−0.03	−2.86	0	0.45	−0.01
N1–C3–C15–N4	−0.78	0.05	0	−24.73	0	1.24	−0.01
N1–C5–C7–N5	−18.97	−0.01	−0.02	−12.94	0	1.79	0
N5–H–N1–C5	–	−0.01	–	–	–	1.66	0.01
C1–N2–H–N6	–	–	–	−2.8	0	–	−0.01
C3–N1–H–N4	–	–	0.01	–	0	1.19	–

Scheme 3

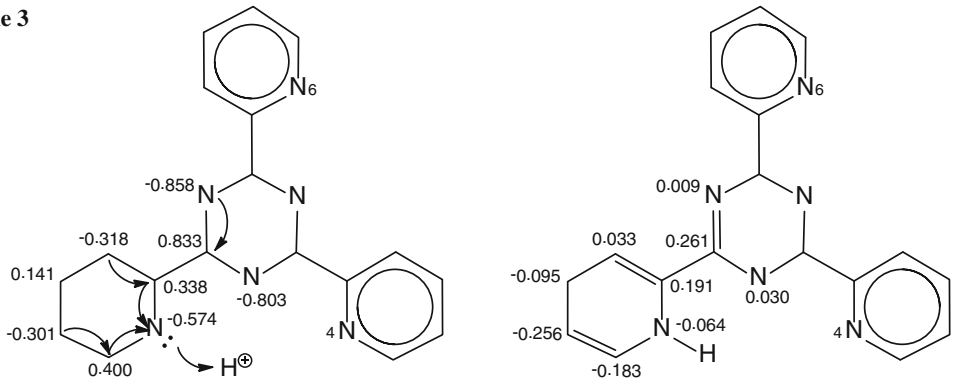

Table 4 Merz-Kollman charges (MK) calculated for TPTZ and the protonated species

Atom	TPTZ	N6	N4	N5	N6,4	N6,5	N4,5
N2	−0.81729	−0.87451	−0.76844	−0.70805	−0.82874	−0.79386	−0.71646
N1	−0.80348	−0.71378	−0.77047	−0.76462	−0.69602	−0.70067	−0.88478
N3	−0.8585	−0.84292	−0.80207	−0.81121	−0.75245	−0.79346	−0.79447
N5	−0.57368	−0.57486	−0.5506	0.020797	−0.52626	−0.018	−0.15246
N4	−0.56409	−0.58393	0.044857	−0.53781	0.040723	−0.54367	−0.14716
N6	−0.53288	−0.07375	−0.55316	−0.53398	−0.12896	−0.11692	−0.51637

leading to two visible transitions at 537 and 593 nm, as can be seen in Fig. 4b. These absorption bands are most likely arising from the outer-sphere charge-transfer (OSCT), $PF_6^- \rightarrow [TPTZH_2]^{2+}$. It is well known that some species, such as *N*-methylpyridinium salts, undergo an OSCT transition in solution [24–26]. The observation of OSCT band is a function of the solvating ability of the solvent.

The photoluminescence properties of TPTZ and $[TPTZH_2](PF_6)_2{\cdot}H_2O$ were studied at room temperature in CH_3CN solution. In the absence of metal ions, the fluorescence of the polypyridyl compounds is probably quenched by the occurrence of a photoinduced electron transfer (PET) process due to the presence of lone pairs of electrons of the N atoms in the pyridyl rings, whereas both the neutral TPTZ molecule and $[TPTZH_2]^{2+}$ cation show fluorescence at the excitation wavelengths of 282 nm for TPTZ, and 274 nm and 598 nm for $[TPTZH_2]^{2+}$ (Fig. 5). The maximum emission peaks of TPTZ are located at 308, 330, and 339 nm. The fluorescence characteristics of the heterocyclic compounds frequently depend on the nature of the solvents used. CH_3CN is a polar solvent and TPTZ tends to be fluorescent in this solvent. UV excitation (282 nm) of the neutral TPTZ molecule populates $^1\pi\pi^*$ and $^1n\pi^*$ excited states. As shown in Fig. 5a, the fluorescence bands show nearly good mirror images of the $\pi \rightarrow \pi^*$ and $n \rightarrow \pi^*$ absorption bands. Consequently, these emission bands are assigned to the $^1(\pi–\pi^*)$ and $^1(n–\pi^*)$ states.

In the fluorescence spectrum of $[TPTZH_2]^{2+}$ (Fig. 5b, c), three bands were observed with their peaks at 358, 373, and 660 nm. These fluorescence bands showed good mirror images of the $\pi \rightarrow \pi^*$, $n \rightarrow \pi^*$, and OSCT absorption bands, so that they were assigned to the fluorescence from the $^1(\pi–\pi^*)$, $^1(n–\pi^*)$, and, e.g., (PF_6^-)-$\pi^*(TPTZH_2^{2+})$ states.

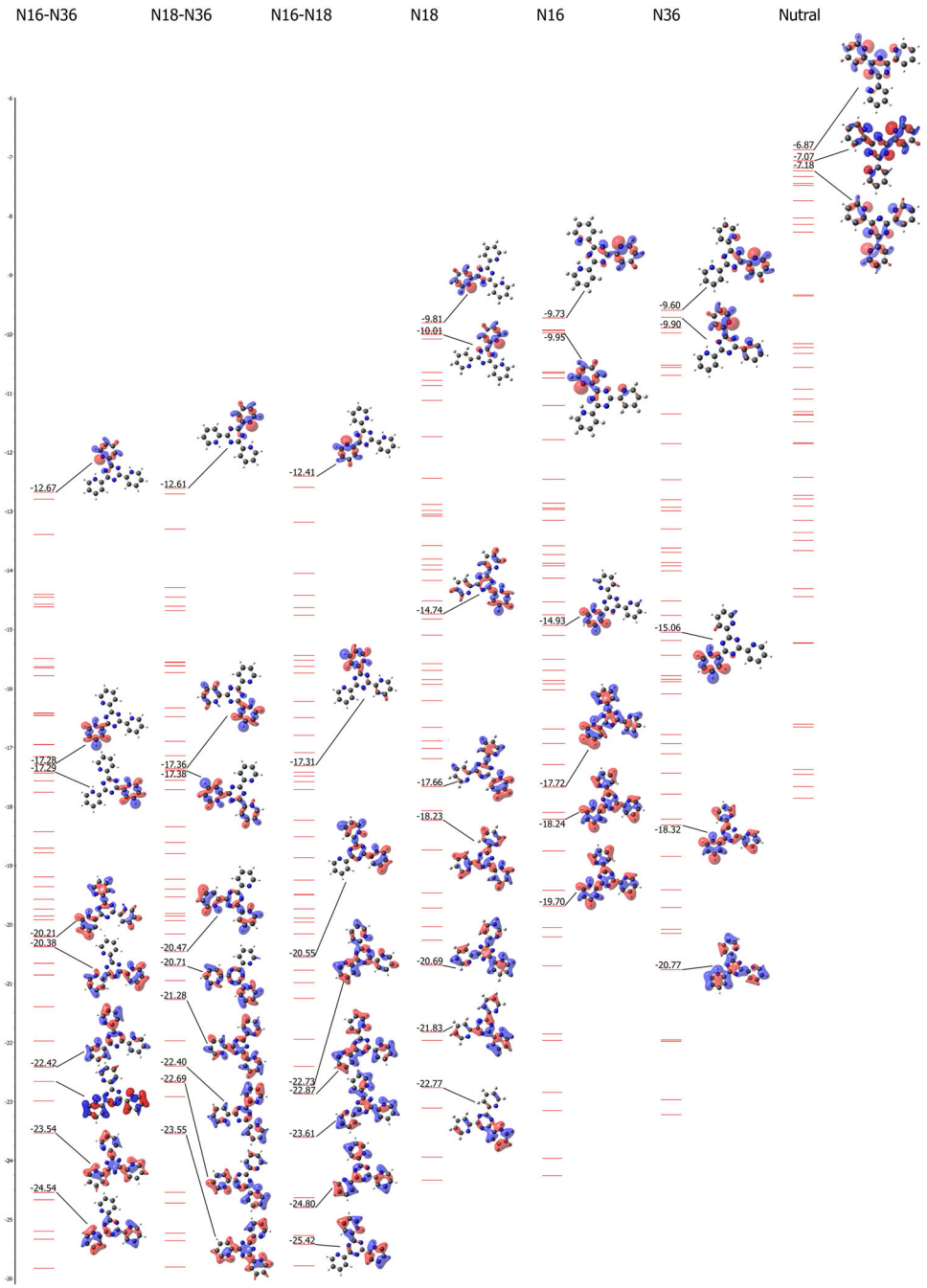

Fig. 1 MO diagram and mportant MOs of TPTZ and its protonated forms

Concluding remarks

1. We have synthesized and characterized the diprotonated 2,4,6-tri(2-pyridyl)-1,3,5-triazine, $[TPTZH_2](PF_6)_2{\cdot}H_2O$. The PF_6^- counterion increases the solubility of the compound in polar organic solvents and resulted in an easier purification.
2. There are two possible conformations for TPTZ (**A** and **B**), which depend on the relative positions of the N atoms in the pyridine rings. Calculations using the 6-31G** basis set have shown that conformation **B** is 11.30 kJ mol^{-1} more stable than conformation **A**.
3. Thermochemical results and the calculated PAs for the first protonation of TPTZ are contradicted by Merz-Kollman atomic charges. The results for the second protonation step were not contradicted by Merz-Kollman atomic charges, and are in agreement with the experimental data.

4. Two visible absorption bands of $[TPTZH_2](PF_6)_2{\cdot}H_2O$ are responsible for the violet color and are most likely arising from the outer-sphere charge-transfer (OSCT).
5. $[TPTZH_2](PF_6)_2{\cdot}H_2O$ displays several fluorescences and can potentially serve as a photoactive material.
6. The molecular $[TPTZH_2]^{2+}$ cation is more planar than the neutral TPTZ molecule.

Table 5 Selected bond lengths/Å and angles/° for $[TPTZH_2](PF_6)_2{\cdot}H_2O$

C1–N2	1.3326 (17)
C1–N3	1.3341 (18)
N2–C3	1.3428 (18)
C3–N1	1.3365 (18)
N1–C5	1.3320 (18)
C5–N3	1.3341 (18)
C7–N5	1.3532 (18)
C21–N6	1.3470 (17)
C25–N6	1.337 (2)
N2–C1–N3	126.53 (13)
N2–C1–C21	116.77 (12)
N3–C1–C21	116.70 (12)
C1–N2–C3	114.38 (12)
N1–C3–N2	124.56 (13)
N1–C3–C15	117.19 (12)
N2–C3–C15	118.24 (12)
C5–N1–C3	114.93 (12)
N1–C5–N3	126.12 (13)
N1–C5–C7	116.75 (12)
N3–C5–C7	117.10 (12)
C5–N3–C1	113.40 (12)
N5–C7–C8	120.09 (13)
N5–C7–C5	116.90 (12)
N6–C21–C22	119.36 (13)
N6–C21–C1	118.09 (12)
N5–C11–C10	120.30 (14)
C11–N5–C7	121.97 (12)
C17–N4–C15	117.53 (12)
N4–C17–C18	123.36 (14)
N6–C25–C24	120.01 (15)
C25–N6–C21	122.66 (13)
HW1–O1–HW2	106 (2)

Experimental

Reagents and measurements

All reagents and solvents used were of reagent grade. Elemental analyses were performed by using a Heraeus CHN-O-Rapid elemental analyzer. The FT-IR spectra were recorded as KBr pellets on a FT-IR JASCO 460 spectrophotometer. Electronic spectra were obtained on a JASCO 7580 spectrophotometer. ^{1}H NMR spectra were recorded on a Bruker Avance DRX-500 MHz spectrometer at an ambient temperature in DMSO-d_6. Fluorescence spectra were taken on a JASCO FP-750 spectrofluorometer. The spectra were measured in CH_3CN solution at room temperature. Solutions were taken in a 1 cm path length fused silica cell.

Computational details

For the computer graphics and the initial construction of the molecular models, we used Gaussview. The models were considered as unprotonated and protonated species, respectively. All calculations were carried out with the GAUSSIAN 03 suite of programs [27]. All structures were optimized at the B3LYP level without imposing any symmetry constraints, using the 6-311+G** basis set. Geometry optimizations were performed without any geometric restrictions using the very tight GAUSSIAN 03 convergence criteria. Frequency calculations were done to ascertain the nature of stationary points on the potential energy surface (PES). Zero-point vibrational energies (ZPVE) calculated at the B3LYP/6-311+G** level were used for all single-point calculations, and the results were scaled by 0.98. The charges were derived from a Chelp population analysis, as

Scheme 4

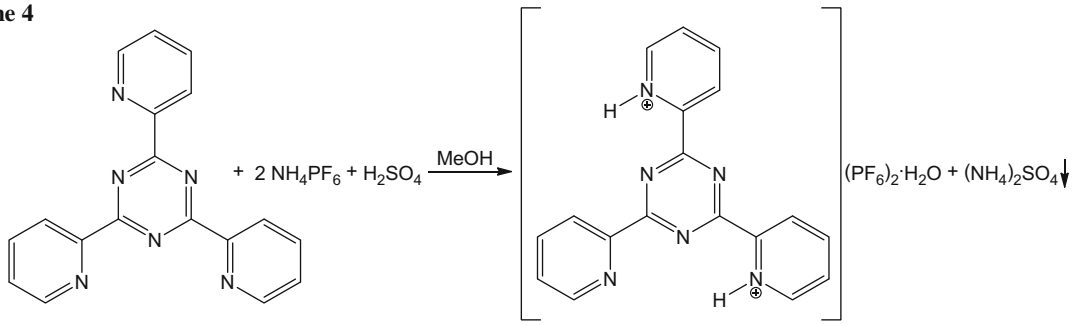

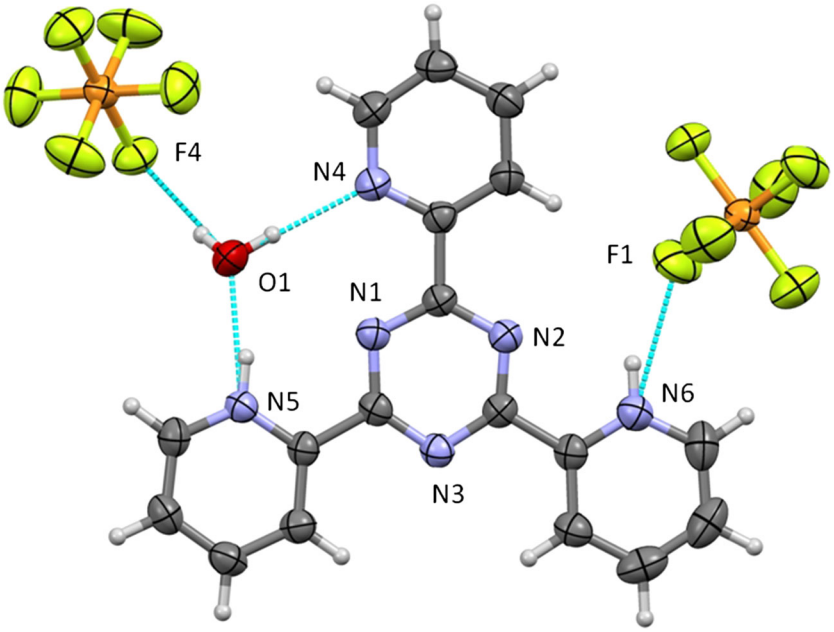

Fig. 2 ORTEP diagram of the $[TPTZH_2]^{2+}$ cation with the H_2O solvent molecule and the two PF_6^- counteranions. Non-H atoms are drawn with displacement ellipsoids at the 90 % probability level, H atoms as spheres with arbitrary radius. *Dotted lines* represent hydrogen bonding interactions

Table 6 Hydrogen bonding geometries with distances/Å and angles/° for $[TPTZH_2](PF_6)_2{\cdot}H_2O$

D–H···A	D···A	H···A	D–H	D–H···A/°
N5–H5N···O1	0.86	1.81	2.6568 (16)	166
N6–H6N···F1^{i}	0.86	2.21	2.9537 (15)	144
O1–HW1···N4	0.86 (3)	2.02 (3)	2.8760 (17)	173 (2)
O1–HW2···F4^{ii}	0.78 (3)	2.15 (3)	2.9167	172 (2)

implemented in the GAUSSIAN 03 program. The gas-phase PA of the species was calculated as the negative standard reaction enthalpy of protonation at 298.15 K:

$$B + H^+ \rightarrow BH^+ PA = -[E_{DFT}(BH^+) - E_{DFT}(B) + (E_{vib}(BH^+) - E_{vib}(B))] + 5/2\,RT,$$

where E_{DFT} is obtained from DFT calculations, E_{vib} includes the zero point energy and temperature corrections to the vibrational enthalpy, and 5/2 RT includes the translational energy of the proton and the Δ(PV) term. The DFT has been reported to be very reliable in calculating PA and in reproducing the experimental results within 1–7 kcal/mol [28].

Two possible conformations for TPTZ (**A** and **B**) are possible, which depend on the relative positions of the N atoms in the pyridine rings. In conformation **A**, in the vicinity of the central ring, different numbers (three, two, or one) of neighboring N atoms are present, while in conformation **B**, the vicinity of the ring contains only two neighboring N atoms in each case (see Scheme 2).

Calculations using the GAUSSIAN94 program [29] were carried out for the two conformations in order to obtain their relative energies. The 6-31G** basis set was used for geometrical optimizations, and it was shown that conformation **B** is 11.30 kJ mol^{-1} more stable than conformation **A**. However, this conformation is found in the

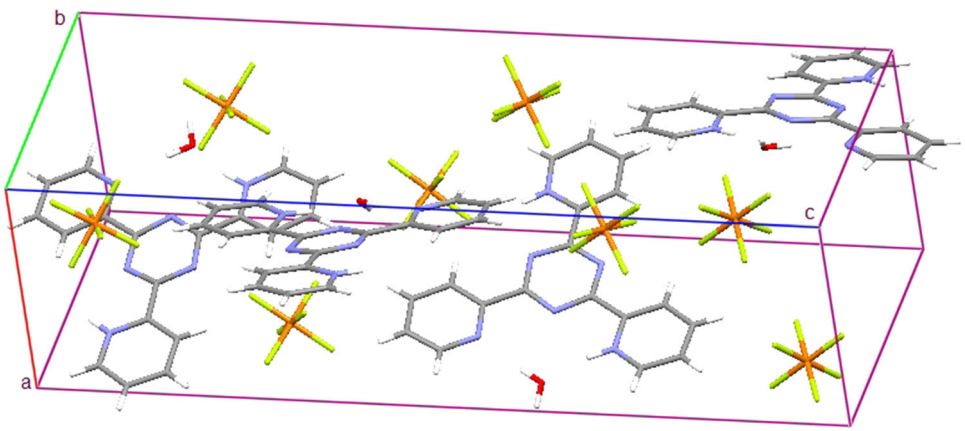

Fig. 3 The packing of the molecular components in the crystal structure of $[TPTZH_2](PF_6)_2{\cdot}H_2O$

Scheme 5

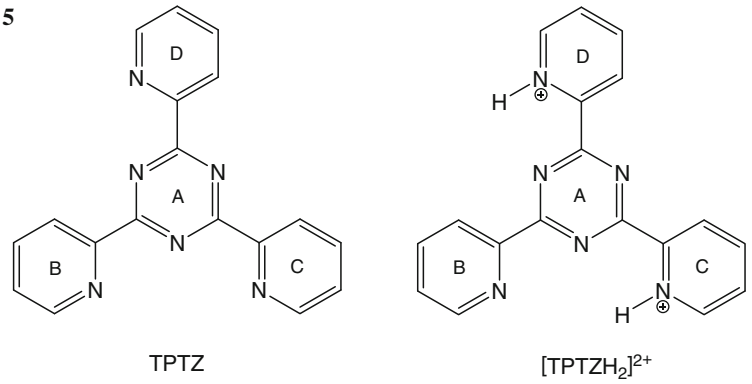

	TPTZ	$[TPTZH_2]^{2+}$
A^D	15.7	6.19
A^C	33.8	7.84
A^B	19.8	3.70

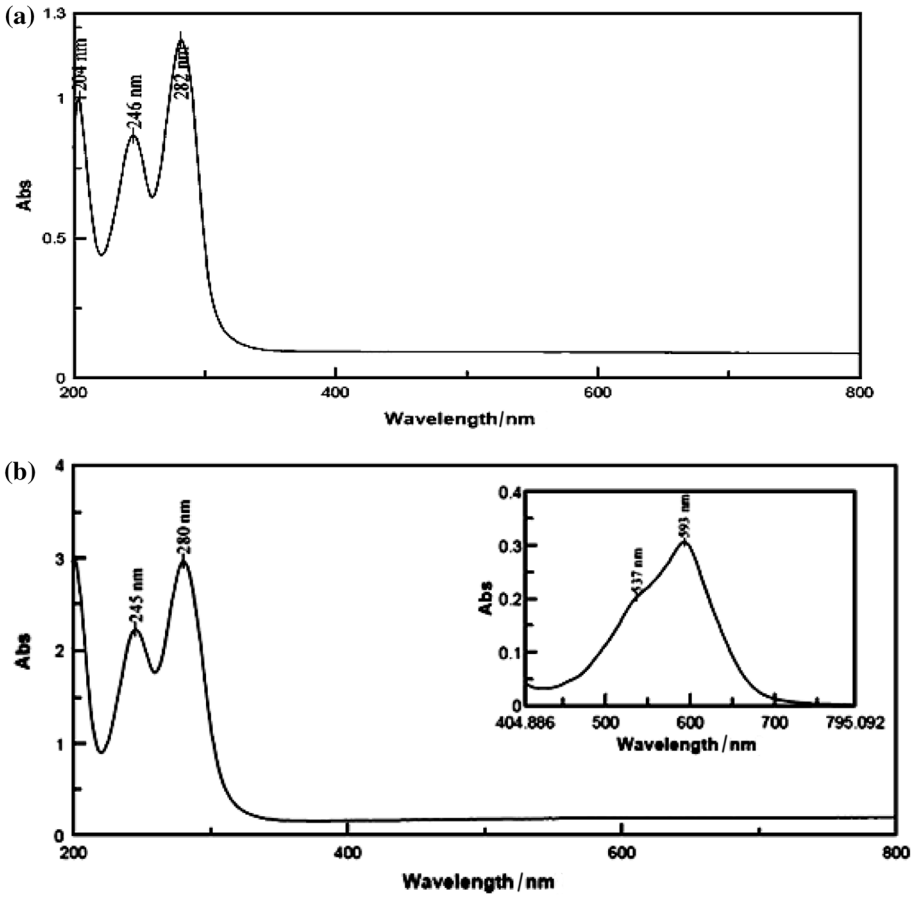

Fig. 4 Electronic spectra of **a** the neutral TPTZ molecule, and **b** $[TPTZH_2](PF_6)_2{\cdot}H_2O$ in CH_3CN

crystal structure of TPTZ [18]. It is interesting that conformation **B** has not been observed in any of the crystal structures of complexes in which TPTZ or its derivatives are coordinated, either with metals or in their protonated forms [30, 31].

With this background information, we used only conformation **A** for all calculations. Scheme 2 represents the atom numbering used for TPTZ, $[TPTZH]^+$, and $[TPTZH_2]^{2+}$. Table 2 reports calculated bond lengths of the optimized molecules at the B3LYP/6-311+G** level.

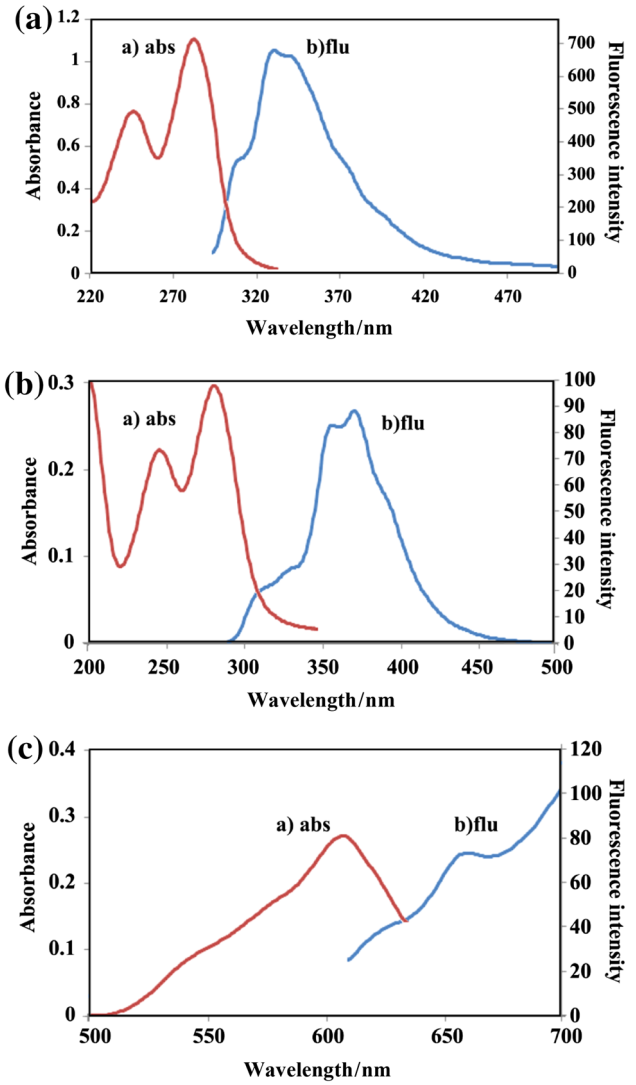

Fig. 5 Absorption (*left*) and fluorescence (*right*) spectra of: **a** TPTZ, **b** and **c** $[TPTZH_2](PF_6)_2{\cdot}H_2O$ in CH_3CN

Table 3 gathers optimized torsion angles of TPTZ and the protonated species.

2,4,6-Tri(2-pyridyl)-1,3,5-triazine bis(hexafluorophosphate) hydrate ($C_{18}H_{16}F_{12}ON_6P_2$)

A mixture of 20 mg TPTZ (0.06 mmol) and 20 mg NH_4PF_6 (0.12 mmol) was added to 10 cm^3 of methanol and stirred at room temperature for 10 min. To the resulting colorless solution, 0.6 cm^3 sulfuric acid (0.1 M) was added dropwise and stirred for 2 h at room temperature. The violet solution was filtered through Celite to remove the fine white $(NH_4)_2SO_4$ precipitate. The violet filtrate was left at room temperature for two days to yield violet crystals. Recrystallization was achieved by slow diffusion of diethyl ether into a saturated solution of the violet crystals in CH_3CN. After three days at room temperature, light violet crystals suitable for X-ray crystallography were formed. Yield: 36 mg (96 %); ^{1}H NMR (500 MHz, DMSO-d_6): δ = 8.99 (dd, 6H, H_a and H_d), 8.29 (t, 3H, H_c), 7.94 (t, 3H, H_b), 7.28 (s, 2H, H_e) ppm; FT-IR (KBr): $\bar{\nu}$ = 3,388 (O–H), 3,316 (N^+–H), 1,539, 1,523, 1,479 (C=N and C=C), 842 (P–F) cm^{-1}; UV–Vis (MeOH): λ_{max} (ε) = 593 (61), 537 (40), 280 (59,360), 245 (44,580) nm (mol^{-1} dm^3 cm^{-1}).

Table 7 Structural data and results of the structure refinements for compound $[TPTZH_2](PF_6)_2{\cdot}H_2O$

Empirical formula	$C_{18}H_{16}F_{12}ON_6P_2$
Formula weight	622.31
Temperature/K	100
Crystal system; space group	Orthorhombic, $P2_12_12_1$
a/Å	8.1695 (9)
b/Å	9.8738 (11)
c/Å	27.952 (3)
V/Å^3	2,254.7 (4)
Z	4
D_x/Mgm^{-3}	1.833
R_{int}	0.023
Crystal size/mm^3	0.6 × 0.2 × 0.1
θ Range for collection/°	2.5–30.0
Index ranges	$-11 \le h \le 9$, $-13 \le k \le 13$, $-39 \le l \le 33$
Reflections collected	28,231
Independent reflections	6,479
Parameters	360
Flack parameter [19]	0.14 (6)
Final R indices $[I > 2\sigma\ (I)]$	0.027, wR_2 = 0.071
Goodness-of-fit on F^2	1.06

X-ray crystallographic study of $[TPTZH_2](PF_6)_2{\cdot}H_2O$

The single crystal measurement was performed on a Bruker-AXS APEXII four-circle diffractometer equipped with a CCD camera. Intensity data were collected using Mo $K\alpha$ radiation (λ = 0.71073 Å). Correction for absorption effects was carried out with the multi-scan approach of SADABS [32]. The crystal structure was solved using direct methods and was refined by the full-matrix least-squares technique on F^2 with the SHELXTL program package [33]. H atoms of the aromatic backbone were positioned geometrically (C–H = 0.93 Å) and were refined as riding with U_{iso}(H) = 1.2U_{eq}(C). The H atoms at the protonated N atoms were clearly discernible from difference maps and were refined with distance restraints N–H = 0.86 Å and U_{iso}(H) = 1.2U_{eq}(N). Water H atoms were also located from difference maps and were refined without restraints. The crystal measured was twinned by inversion with a refined twin component ratio of 0.86 (6):

0.14 (6). Selected bond lengths and angles of $[TPTZH_2](PF_6)_2{\cdot}H_2O$ are gathered in Table 5. Also details of hydrogen bonding geometries of $[TPTZH_2](PF_6)_2{\cdot}H_2O$ are given in Table 6. Crystallographic data and details of data collection and structure refinement are listed in Table 7. Crystallographic data has been deposited with the Cambridge Crystallographic Data Centre, CCDC No. 832783.

Acknowledgments We are grateful to the Isfahan University of Technology (IUT) for financial support.

References

1. Gray HB, Stiefel EI, Valentine JS, Bertini I (eds) (2007) Biological inorganic chemistry: structure and reactivity. University Science Book, Sausalito
2. Fernandes I, Faria A, Azevedo J, Soares S, Calhau C, De Freitas V, Mateus N (2010) J Agric Food Chem 58:3785
3. Katritzky AR (2004) Chem Rev 104:2125
4. Stambasky J, Hocek M, Kočovský P (2009) Chem Rev 109:6729
5. Süleymanoğlu N, Ustabaş R, Alpaslan YB, Ünver Y, Turan M, Sancak K (2011) J Mol Struct 989:101
6. Khan MTH (ed) (2007) Bioactive heterocycles IV; topics in heterocyclic chemistry, vol 10. Springer, Berlin
7. Eicher T, Hauptmann S (2003) The chemistry of heterocycles: structure, reactions, syntheses, and applications. Wiley-VCH, Weinheim. http://www.amazon.com/Chemistry-Heterocycles-Structure-Reactions-Applications/dp/3527307206
8. Bei F-L, Yang X-J, Lu L-D, Wang X (2004) J Mol Struct 689:237
9. Hwang S, Jang YH, Chung DS (2005) Bull Korean Chem Soc 26:585
10. Huang H, Rodgers MT (2002) J Phys Chem A 106:4277
11. Schmiedekamp M, Topol IA, Christopher JM (1995) Theor Chim Acta 92:83
12. Gutmann V (1975) Coord Chem Rev 15:207
13. Gutmann V (1976) Coord Chem Rev 18:225
14. Allen FH, Motherwell WDS (2002) Acta Crystallogr B 58:407
15. Gilli G, Gilli P (2000) J Mol Struct 552:1
16. Bond AD, Jones W (2002) Supramolecular organization, Materials Design. Cambridge University Press, Cambridge
17. Desiraju GR (2003) Crystal design: structure and function. Wiley, Chichester
18. Drew MGB, Hudson MJ, Iveson PB, Russell ML, Madic C (1998) Acta Crystallogr C 54:985
19. Janczak J, Śledź M, Kubiak R (2003) J Mol Struct 659:71
20. Nakamato K (1997) Infrared and raman spectra of inorganic and coordination compounds, part II: application in coordination, organometallic, and bioinorganic chemistry, 5th edn. Wiley-Interscience, New York
21. Ruminski RR, Letner C (1989) Inorg Chim Acta 162:175
22. Hadadzadeh H, Hosseinian SR, Fatemi SJA (2009) Polyhedron 28:2776
23. Paul P, Tyagi B, Bilakhiya AK, Bhadbhade MM, Suresh E, Ramachandraiah G (1998) Inorg Chem 37:5733
24. Drago RS (1992) Physical methods for chemists, 2nd edn. Saunders, Philadelphia
25. Kunkely H, Vogler A (2004) Inorg Chim Acta 357:1292
26. Kunkely H, Vogler A (2000) Inorg Chim Acta 310:279
27. Frisch MJ, Trucks GW, Schlegel HB, Scuseria GE, Robb MA, Cheeseman JR, Montgomery JA Jr, Vreven T, Kudin KN, Burant JC, Millam JM, Iyengar SS, Tomasi J, Barone V, Mennucci B, Cossi M, Scalmani G, Rega N, Petersson GA, Nakatsuji H, Hada M, Ehara M, Toyota K, Fukuda R, Hasegawa J, Ishida M, Nakajima T, Honda Y, Kitao O, Nakai H, Klene M, Li X, Knox JE, Hratchian HP, Cross JB, Bakken V, Adamo C, Jaramillo J, Gomperts R, Stratmann RE, Yazyev O, Austin AJ, Cammi R, Pomelli C, Ochterski JW, Ayala PY, Morokuma K, Voth GA, Salvador P, Dannenberg JJ, Zakrzewski VG, Dapprich S, Daniels AD, Strain MC, Farkas O, Malick DK, Rabuck AD, Raghavachari K, Foresman JB, Ortiz JV, Cui Q, Baboul AG, Clifford S, Cioslowski J, Stefanov BB, Liu G, Liashenko A, Piskorz P, Komaromi I, Martin RL, Fox DJ, Keith T, Al-Laham MA, Peng CY, Nanayakkara A, Challacombe M, Gill PMW, Johnson B, Chen W, Wong MW, Gonzalez C, Pople JA (2003) Gaussian 03, Revision A,1. Gaussian Inc, Pittsburgh
28. Fitzgerald G, Andzelm J (1991) J Phys Chem 95:10531
29. Frisch MJ, Trucks GW, Schlegel HB, Gill PMW, Johnson BG, Robb MA, Cheeseman JR, Keith TA, Petersson GA, Montgomery JA Jr, Raghavachari K, Al-Laham MA, Zakrzewski VG, Ortiz JV, Foresman JB, Cioslowski J, Stefanov BB, Nanayakkara A, Challalcombe M, Peng CY, Ayala PY, Chen W, Wong MW, Andrews JL, Replogle ES, Gomperts R, Martin RL, Fox DL, Binkley JS, Defrees DJ, Baker J, Stewart JP, Head-Gordon M, Gonzalez C, Pople JA (1995) Gaussian 94, Revision A.1. Gaussian Inc, Pittsburgh
30. Barclay GA, Vagg RS, Watton EC (1977) Acta Crystallogr B 33:3487
31. Chan GYS, Drew MGB, Hudson MJ, Isaacs NS, Byers P (1996) Polyhedron 15:3385
32. SADABS (2008) A Program for Empirical Absorption and other Corrections. Bruker AXS Inc, Madison
33. Sheldrick GM (2008) Acta Crystallogr A 64:112